STEERING CONTROL OF AN UNDERWATER VEHICLE : AN ANTI-WINDUP DESIGN

Jean-Pierre Folcher
Laboratoire Informatique Signaux et Systèmes de Sophia Antipolis
Route des Lucioles, Sophia-Antipolis, France
folcher@i3s.unice.fr

Abstract

In this paper, a synthesis approach based on the anti-windup control will be developped. The proposed approach consists in designing a nominal controller and then adding an extra anti-wind up compensator which ensures the absolute stability of the closed loop system against sector bounded nonlinearity. This approach is applied to design the steering control system for the ROV Phanthom 500.

1 Introduction

Linear systems with input nonlinearities occur very often in practice. A typical example is an underwater vehicle with speed saturated thrusters. In the control loop their effect is that the actual command input of the system differs from the controller output. In some cases, the propeller nonlinearity may be neglected while in other their effect may be considerable, leading to instability or performance degradation if ignored when designing the controller. In many designs, the saturation problem is implicitly taken into account with numerous synthesis steps and extensive simulations to check that the actuators never saturate. These approaches involve numerous trial and error synthesis/validation iterations but lead to prohibitive design time. To ensure the global stability of the closed loop system, the designed controller often induces poor control performances.

An alternative is a two step design procedure. A nominal linear controller which ensures tight closed loop system performance for the system neglecting the nonlinearity is synthesized. Then an anti-windup compensator is designed such that :

- when the system does not saturate, the response coincides with the linear unconstrained response ;
- when the nonlinearity is "excited", the closed loop stability is ensured and the performance objective is kept at an acceptable level.

The objective of this paper is to propose a simple anti-windup design method ensuring local stability and performance (reference tracking, disturbance rejection) for a linear system with sector nonlinearities. The proposed method is strongly related to absolute stability problem and is based on the local version of the standard Circle Criterion. This anti-windup control method is applied to design the steering controller of the Remotely Operated Vehicle (ROV) Phantom 500. The advantages of the proposed control design technique are demonstrated.

2 Steering Control Problem of an Underwater Vehicle with Speed Speed Saturated Thrusters

In this paper we study the control system for a Phantom 500 underwater robot. The Phantom 500 vehicle [1] has an open frame structure (see figure 1). This ROV is actuated by two horizontal thrusters for surge and yaw motion, and a vertical thruster for heave motion. Roll and pitch dynamics are not controlled but are intrinsically stable.

[1] Phantom is an underwater robot produced by Deep Ocean Engineering, Palo Alto, USA. This vehicle is used in the research projects of the *Laboratoire d'Informatique, Signaux et Systèmes de Sophia Antipolis (I3S)* through a special education/research arrangement.

Figure 1: Phantom 500 underwater vehicle.

For the purposes of on-board sensor based-identification and of control design we consider three non-interacting (or lightly interacting) dynamics for the surge speed motion, the steering motion and the diving motion. In the sequel we consider only motion of the underwater vehicle in the horizontal plane.

The steering and the longitudinal speed models are derived from the general Newton-Equation expressed in the body reference frame. The interested reader is refered to [4] for futher details on the modeling aspects. The surge motion is described by the following transfert function

$$\frac{u(s)}{a_u(s)} = \frac{1}{\alpha_u s + 1}\ , \tag{1}$$

where u is surge speed and a_u is surge acceleration. The heading dynamics is modelled as

$$\frac{\psi(s)}{r(s)} = \frac{1}{s}\ , \quad \frac{r(s)}{a_r(s)} = \frac{1}{\alpha_r s + 1}\ , \tag{2}$$

where ψ is heading angle, r is yaw rate speed, and a_r rate acceleration. In many standard operating conditions, the propeller trust can be expressed as $\tau = c_\tau n|n|$ where n is the propeller rotation speed. Thus, considering a vehicle equipped with a left thruster and a right thruster the surge and rate accelerations can be written

$$\begin{aligned} a_u &= \delta_{ul}|n_l|n_l + \delta_{ur}|n_r|n_r, \\ a_r &= \delta_{rl}|n_l|n_l + \delta_{rr}|n_r|n_r, \end{aligned} \tag{3}$$

where n_l is the left propeller rotation speed and n_r is the right propeller rotation speed. Parameters δ_{ul}, δ_{ur}, δ_{rl} and δ_{rr} depends on c_τ and geometric characteristics of the vehicle. The vehicle motion in the horizontal plane is described by equations (1), (2) and (3).

The model parameters values were obtained using a maximum likelihood identification method, see [2]

$$\begin{bmatrix} \alpha_r \\ \delta_{rl} \\ \delta_{rr} \end{bmatrix} = \begin{bmatrix} 0.75 & \\ -6.21 & 10^{-6} \\ -5.74 & 10^{-6} \end{bmatrix},$$

$$\begin{bmatrix} \alpha_u \\ \delta_{ul} \\ \delta_{ur} \end{bmatrix} = \begin{bmatrix} 0.44 & \\ 2.74 & 10^{-5} \\ -1.04 & 10^{-5} \end{bmatrix}.$$

Note that the plant nonlinear behaviour is induced by the propellers characteristics, see (3). The input static nonlinearities of these two plants can be cancelled using a static feedforward precompensator which computes the required propeller speeds

$$\begin{aligned} n_l^r &= sign\left(\frac{\delta_{ur}a_r^r - \delta_{rr}a_u^r}{\delta_{ur}\delta_{rl} - \delta_{rr}\delta_{ul}}\right)\sqrt{\left|\frac{\delta_{ur}a_r^r - \delta_{rr}a_u^r}{\delta_{ur}\delta_{rl} - \delta_{rr}\delta_{ul}}\right|}, \\ n_r^r &= sign\left(\frac{\delta_{ul}a_r^r - \delta_{rl}a_u^r}{\delta_{ul}\delta_{rr} - \delta_{rl}\delta_{ur}}\right)\sqrt{\left|\frac{\delta_{ul}a_r^r - \delta_{rl}a_u^r}{\delta_{ul}\delta_{rr} - \delta_{rl}\delta_{ur}}\right|}, \end{aligned} \tag{4}$$

from the required accelerations a_u^r and a_r^r. This is an input linearisation technique, see [7]. The left and right propellers are speed controlled, see [2]. This approach is valid if we assume that the speed controlled propeller dynamics is faster than the horizontal motion dynamics (time-scale separation principle). The horizontal plane motion of the Phantom 500 with the precompensator is shown in figure 2. Thus, the precompensator in series with the plant is approximated by two linear decoupled models given by (1), (2) where $a_u^r \rightarrow a_u$ and $a_r^r \rightarrow a_r$. Saturation phenomenon acting on the propellers speed (propeller speed is limited in magnitude to $n_{sat} = 1000\ rpm$) induces input static nonlinearities for the global dynamics. In the sequel of the paper, we consider only the control problem for the heading motion and consequently we fix $a_u^r = 0$. For the sake of simplicity we set $u = a_r^r$ and the induced input nonlinearity

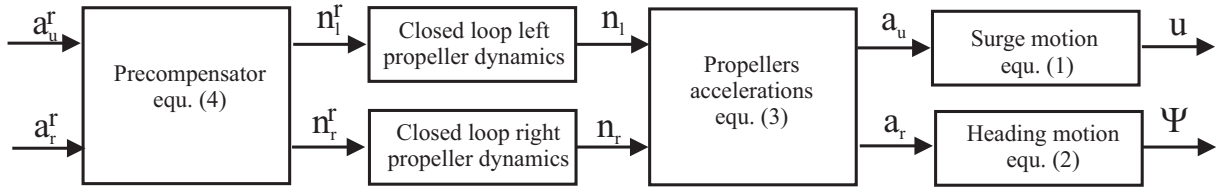

Figure 2: Surge and heading dynamics with the precompensator.

$v = a_r = \varphi(u)$ is defined as follows:

$$\begin{array}{ll} u \le -u_2 & \varphi(u) = -\varphi_{sat}, \\ -u_2 < u < -u_1 & \varphi(u) = -u_1 + \alpha(u + u_1), \\ -u_1 \le u \le u_1 & \varphi(u) = u, \\ u_1 < u < u_2 & \varphi(u) = u_1 + \alpha(u - u_1), \\ u \ge u_2 & \varphi(u) = \varphi_{sat}. \end{array} \tag{5}$$

The parameters of φ are

$$\begin{aligned} u_1 &= \frac{|\delta_{ur}\delta_{rl} - \delta_{rr}\delta_{ul}|}{\max\left(|\delta_{ur}|, |\delta_{ul}|\right)} n_{sat}^2, \\ u_2 &= \frac{|\delta_{ur}\delta_{rl} - \delta_{rr}\delta_{ul}|}{\min\left(|\delta_{ur}|, |\delta_{ul}|\right)} n_{sat}^2, \\ \psi_{sat} &= \left(|\delta_{rl}| + |\delta_{rr}|\right) n_{sat}^2, \\ \alpha &= \frac{\varphi_{sat} - u_1}{u_2 - u_1}. \end{aligned}$$

In summary, the heading dynamics controlled by the static precompensator is described by

$$v = \varphi(u), \tag{6}$$

and

$$\frac{\psi(s)}{v(s)}, \ = \frac{1}{p(\alpha_r s + 1)} \ . \tag{7}$$

In the sequel we will design the linear controller for the system defined by (6), (7). This system is a linear system subject to an input nonlinearity as depicted on figure 3.

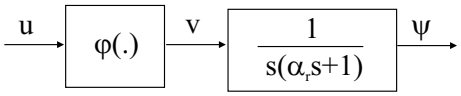

Figure 3: Linear system subject to an input nonlinearity.

3 Stability analysis

In this section we consider a system represented as a feedback connection of a linear dynamical system (defined by transfert function T_{qp}) and a nonlinear function φ as shown in figure 4.

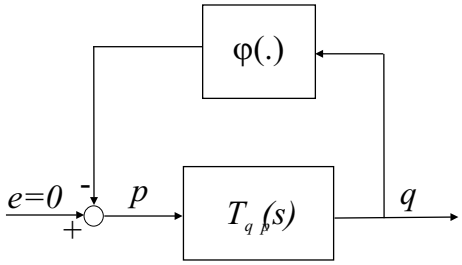

Figure 4: Linear system and a nonlinear interconnection.

$T_{qp}(s)$ is a stricty proper single-input single-output transfer function. $\varphi(.)$ is a memoryless, possibly time-varying, nonlinearity which is piecewise continuous in t and locally Lipchitz in y. The nonlinearity φ is required to satisfy the following sector condition $[a\ b]$:

$$(\varphi(t,q) - aq)\,(\varphi(t,q) - bq) \le 0, \ \ \forall t \ge 0, \ \forall q \in [\alpha\ \beta]. \tag{8}$$

The nonlinearity defined in (5) is plotted in figure 5. Note that if $|u(t)| \le u_{max}$ with $u_{max} > u_2$, then φ belongs to the sector $[\psi_{sat}/u_{max}\ 1]$.

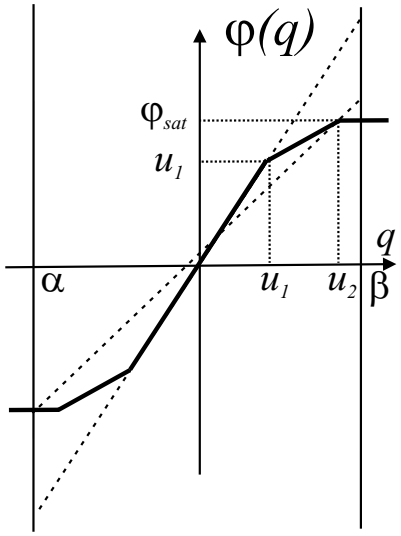

Figure 5: Static input nonlinearity.

Theorem (Circle Criterion, [6]). *Consider an interconnected system (T_{qp}, φ) where $T_{qp}(p)$ describes the linear part, and nonlinear function φ satisfies the sector condition (8) on the interval $[\alpha\ \beta]$. Then the system is absolutely stable if one of the following conditions is satisfied, as appropriate:*

1. *If $0 < a < b$, the Nyquist plot of $T_{qp}(j\omega)$ does not enter the disk $D(a, b)$ and encircles it m times in the counterclockwise direction, where m is the number of poles of $T_{qp}(s)$ with positive real parts.*
2. *If $0 = a < b$, $T_{qp}(p)$ is Hurwitz and the Nyquist plot of $T_{qp}(j\omega)$ lies to the right of the line $s = -1/b$.*
3. *If $a < 0 < b$, $T_{qp}(p)$ is Hurwitz and the Nyquist plot of $T_{qp}(j\omega)$ lies in the interior of the disk $D(a, b)$.*

The Circle Criterion allows to analyse the absolute stablility using only the Nyquist plot of $T_{qp}(p)$. This criterion will be use to analyse the stability of the closed loop system in the sequel of this paper in section 5.

4 Nominal controller design

In this section, we suppose that for a given reference signal ψ_r we have

$$|u(t)| \leq u_{max}.$$

In this context, $v = \psi(u) = u$ and the system defined by (6), (7) reduces to the linear part (7).

Under this assumption we can consider the classical feedback loop show in figure 6.

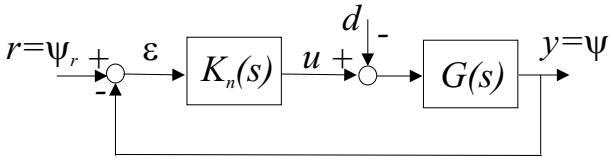

Figure 6: Nominal closed loop control problem.

$K_n(s)$ is the linear part of the controller and $G(p)$ is the transfer function describing the heading dynamics in series with the precompensator. Signals $r = \psi_r$ and d are, respectively, the reference signal and the input perturbation signal ; u is the input command signal ; ϵ is the error signal and $y = \psi$ is the measured output. Our objective is to determine $K_n(s)$ using a robust design method based on $\mathbf{H}_\infty$ optimisation. This approach is strongly related to classical synthesis methods. $\mathbf{H}_\infty$-based design methods were previously applied to AUV control in [1], [5], [3]. The key point of the approach consists in shaping the main closed loop transfer functions defined as

$$\begin{bmatrix} \epsilon(s) \\ u(s) \end{bmatrix} = \begin{bmatrix} \frac{1}{1+G(s)K(s)} & \frac{G(s)}{1+G(s)K(s)} \\ \frac{K(s)}{1+G(s)K(s)} & \frac{K(s)G(s)}{1+G(s)K(s)} \end{bmatrix} \begin{bmatrix} r(s) \\ d(s) \end{bmatrix},$$
$$= \begin{bmatrix} T_{\epsilon r}(s) & T_{\epsilon d}(s) \\ T_{ur}(s) & T_{ud}(s) \end{bmatrix} \begin{bmatrix} r(s) \\ d(s) \end{bmatrix}.$$

The closed loop system behavior is entirely determined by the four different (closed-loop) transfer functions $T_{\epsilon r}(s)$, $T_{\epsilon d}(s)$, $T_{ur}(s)$, and $T_{ud}(s)$. Examination of the frequency responses provides some crucial information about the closed loop system properties, see [3]. We choose the convenient synthesis framework illustrated in figure 7

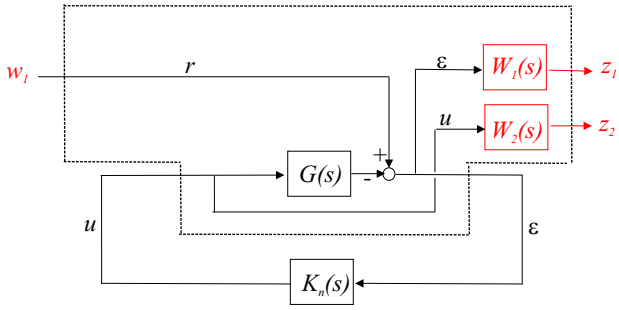

Figure 7: K_n synthesis problem: an $\mathbf{H}_\infty$ standard representation.

This block diagram represents the *Standard* $\mathbf{H}_\infty$ *Synthesis Problem*. Let $T_{zw}(s)$ be the transfer matrix between z and w in figure 7. The synthesis objectives are :

- to ensure closed loop stability,
- to fix a gain between the input w and the output z for a fixed value γ : $\|T_{zw}(s)\|_\infty < \gamma$.

Its numerical solution is based on the Glover and Doyle algorithm presented in [5] and involves the resolution of two Riccati equations. We seek a controller K_n that stabilizes the closed loop system and ensures that the $\mathbf{H}_\infty$ norm of transfer matrix $T_{zw}(s)$ is bounded by one :

$$\|T_{zw}(s)\|_\infty = \left\| \begin{array}{c} W_1(s)T_{\epsilon r}(s) \\ W_2(s)T_{ur}(s) \end{array} \right\|_\infty < \gamma$$

If the previous inequality is enforced, then every block of the transfer matrix $T_{zw}(s)$ has a norm bounded by one. We obtain for all frequencies ω

$$\begin{array}{rcl} |T_{\epsilon r}(j\omega)| & < & \gamma\,|W_1(j\omega)|^{-1}, \\ |T_{ur}(j\omega)| & < & \gamma\,|W_2(j\omega)|^{-1}. \end{array}$$

The choice of the weighting functions $W_1(s)$ and $W_2(s)$ allows to shape two closed loop transfer functions. The weighting functions were fixed to

$$\begin{array}{rcl} W_1(s) & = & 0.5\left(\dfrac{s+0.5}{s+5\ 10^{-4}}\right)^2, \\ W_2(s) & = & 10^{-6}\left(\dfrac{s+10}{s+1000}\right)^3. \end{array}$$

The choice of $W_1(s)$ leads to a reasonable bandwidth, ensures a modulus margin of $1/2$ and guarantees a relative steady state error less that 10^{-3}. Choice of $W_2(s)$ allows to decrease the controller magnitude for large frequencies. Extra dynamics of the designed controller which are not necessary to control the plant where removed. We obtain a second order controller with transfer function

$$K_n(s) = -6.66\ 10^{-2}\,\frac{(s+1.71)(s-7.54)}{(s+0.84)^2+(1.81^2)},$$

and $\gamma = 0.92$. Figure 8 shows the Bode diagram of the closed loop transfer function $T_{\epsilon r}(s)$ and the template $W_1(s)^{-1}$. The weighting function shapes the closed loop transfer function in the low frequencies domain and ensures a correct modulus margin, and a bandwidth of $0.4\ rd/s$. The frequency response of the closed loop transfer function $T_{ur}(s)$ and of the template $W_2(s)^{-1}$ are plotted in Fig 9. Remark that the weighting function shapes the closed loop transfer function in the high frequency domain and ensures a correct input command level.

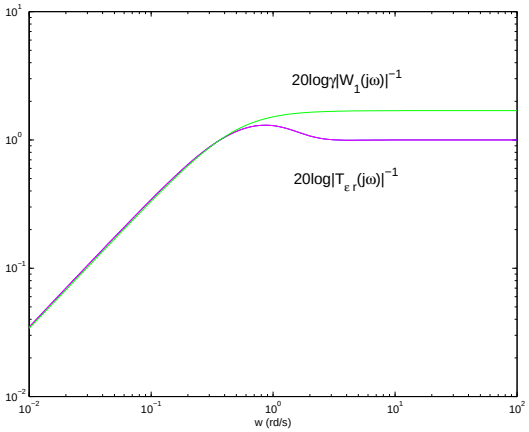

Figure 8: Sensitivity performance ($T_{\epsilon r}(s)$ and $W_1(s)^{-1}$ Bode diagram).

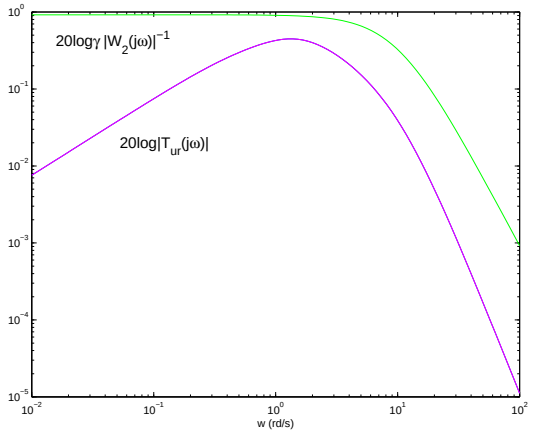

Figure 9: Control bandwidth ($T_{ur}(s)$ and $W_2(s)^{-1}$ Bode diagram).

5 Anti-windup controller design

In this section we propose the anti-windup control structure shown in figure 10. Comparing to the closed loop drawn in figure 6, the nonlinearity bloc is taken into account. The objective is to design the anti-windup compensator $K_{aw}(p)$ ensuring absolute stability for the sector nonlinearity. We have considered that the nonlinearity φ is in the sector $[a\ b]$. In order to recast this synthesis problem into a systematic $\mathbf{H}_\infty$ based design, the loop transformation shown in figure 10 is performed, where

$$\Gamma = \frac{b-a}{2}, \quad \Gamma = \frac{a+b}{2}.$$

This interconnection has to be compared with the feedback connection of a linear dynamical system and a nonlinear function as shown in figure 4. $-\bar{T}_{qp}$ represents the linear part of the closed loop, excluding the nonlinearity φ. This loop transformation leads to the new nonlinearity

$$\bar{\varphi}(\bar{q}) = \Pi_{-1}\left(\varphi(\bar{q}) - \Gamma\bar{q}\right)\big|_{q=\tilde{q}}$$

residing in sector $[-1\ 1]$. The loop shifted linear part of the system becomes

$$\bar{T}_{\bar{q}\bar{p}}(s) = \left(1 + \bar{T}_{qp}(s)\Gamma\right)^{-1} T_{qp}(s)\Pi.$$

To ensure absolute stability (see Theorem in section 3), $\bar{T}_{\bar{q}\bar{p}}(s)$ has to be Hurwitz and the Nyquist plot of $\bar{T}_{\bar{q}\bar{p}}(s)$ must lie in the interior of the disk $D(-1,1)$, which imposes that

$$\left\|\bar{T}_{\bar{q}\bar{p}}(s)\right\|_\infty < 1.$$

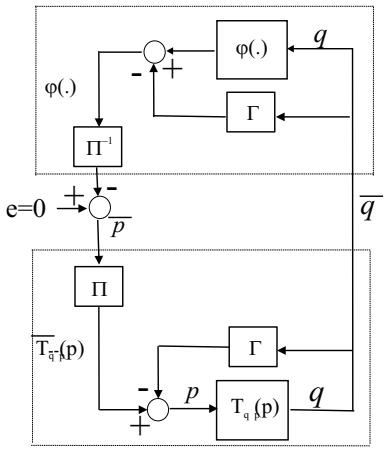

Figure 11: A loop transformation.

$\mathbf{H}_\infty$ standard synthesis framework can be used to ensure this frequency constraint and to shape closed loop transfer function. A convenient synthesis block diagram is shown in figure 12.

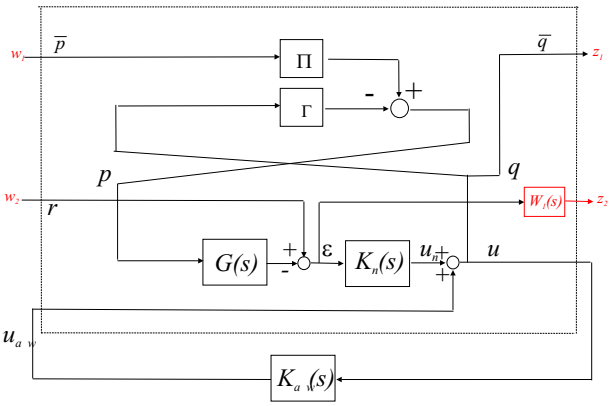

Figure 12: K_{aw} synthesis problem: an $\mathbf{H}_\infty$ standard representation.

Let $\bar{T}_{zw}(s)$ be the transfer matrix between z and w in figure 12. We seek a controller transfer function K_{aw} that

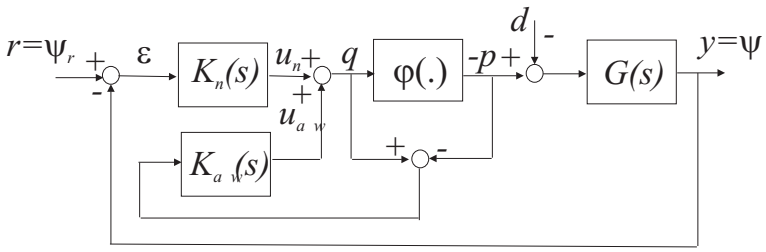

Figure 10: Anti-windup controller structure.

stabilizes the closed loop system and ensures that the $\mathbf{H}_\infty$ norm of transfer matrix $\bar{T}_{zw}(s)$ is bounded by $\bar{\gamma}$:

$$\|\bar{T}_{zw}(s)\|_\infty = \left\| \begin{array}{cc} \bar{T}_{\tilde{q}\bar{p}}(s) & T_{\bar{q}r}(s) \\ \bar{W}_1(s)\bar{T}_{\epsilon\bar{p}}(s) & \bar{W}_1(s)\bar{T}_{\epsilon r}(s) \end{array} \right\|_\infty < \bar{\gamma}$$

If the previous inequality is enforced, then

$$\left\|\bar{T}_{\tilde{q}\bar{p}}(p)\right\|_\infty < \bar{\gamma},$$

which ensures absolute stability for the closed loop if $\bar{\gamma} \leq 1$. Moreover

$$\left\|\bar{W}_1(s)\bar{T}_{\epsilon r}(s)\right\|_\infty < \bar{\gamma},$$

and the choice of the weighting functions $\bar{W}_1(s)$ allows to shape the sensitivity transfer function $\bar{T}_{\epsilon r}(s)$ in the same way as in section 4. We obtain for all frequencies ω

$$\left|\bar{T}_{\epsilon r}(j\omega)\right| < \bar{\gamma}\left|\bar{W}_1(j\omega)\right|^{-1}.$$

The performance weighting function is fixed to

$$\bar{W}_1(s) = 0.34\left(\frac{s+0.001}{s+0.5}\right)^2,$$

and the consider that φ is in sector $[0.1\ 1]$, i.e. $u_{max} = 10\varphi_{sat}$. The designed controller has extra dynamics which are not necessary to control the plant. These extra states are removed using controller reduction models based on balanced state space representation and controllability and observability grammians. We obtain a second order controller with transfer function

$$K_{aw}(s) = 1.14\frac{(s+0.59)(s+2.22)}{(s+0.47)(s+3.21)},$$

and $\bar{\gamma} = 0.98$. We can check in figure 13 that for all frequencies ω whe have $\left|\bar{T}_{\tilde{q}\bar{p}}(j\omega)\right| < 1$.

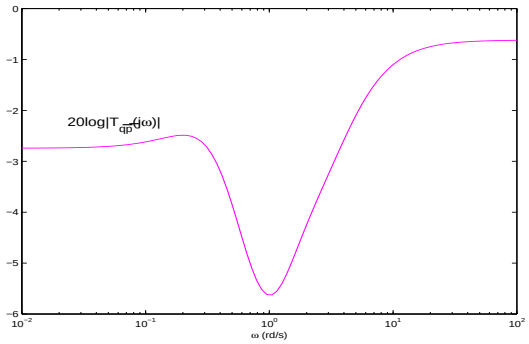

Figure 13: $\bar{T}_{\tilde{q}\tilde{p}}(s)$ Bode diagram.

The absolute stability is ensured for the interconnection $(\bar{T}_{\tilde{q}\tilde{p}}, \bar{\varphi})$. It implies (loop transformation) that the interconnection $(\bar{T}_{qp}, \varphi)$ is also absolutely stable.

To evaluate the loop performance, we consider the transfer function $\bar{T}^k_{\epsilon r}(s)$ which describes the relation between the reference input signal r and the output error signal ϵ defined in figure 10 when the nonlinearity reduces to a simple gain k, i.e. $\varphi(q) = kq$. Note that for the case $k = 0$ we obtain $\bar{T}^0_{\epsilon r}(s) = \bar{T}_{\epsilon r}(s)$. Fig 14 shows the Bode diagram of the closed loop transfer functions $\bar{T}^k_{\epsilon r}(s)$ for selected values of $k \in [a\ b]$ and the template $\bar{\gamma}\bar{W}_1(s)^{-1}$. We can check that the sensitivity performance is ensured *robustly*: for all values of $k \in [a\ b]$ the following frequency constraint (for all frequencies ω) is ensured $\left|T^k_{\epsilon r}(j\omega)\right| < \bar{\gamma}\left|\bar{W}_1(j\omega)\right|^{-1}$. The loop bandwidth is about $0.4\ rd/s$ and the modulus margin is $MM = 1/2$.

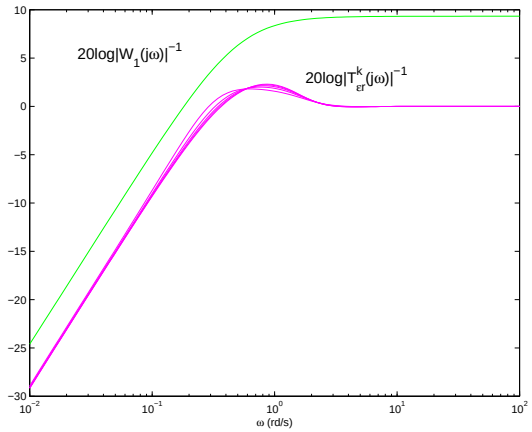

Figure 14: Sensitivity performance : $\bar{T}^k_{\epsilon r}(s)$ and $\bar{\gamma}\bar{W}_1(s)^{-1}$ Bode diagram.

Figure 15 shows the heading ψ time response for the closed loop system shown in figure 10. The magnitude of the reference step is $180°$. The achieved setting time is $16\ s$ and there is no overshoot. The command input u time response is plotted in figure 16. Note that the signal u_{aw} is zero when the nonlinearity is not 'excited', i.e. when $|u(t)| < u_1$.

6 Concluding remarks

In this paper we presented the design of the steering controller of an underwater vehicle subject to speed saturated propellers nonlinearities. Neglecting the speed saturation, an input linearization technique allows to obtain a precompensator which linearizes the surge and heading dynamics. By taking into account the speed saturation phenomena, the aggregated system (precompensator with the surge and heading dynamics) includes a sector bounded non linearity. The linear part of the steering control system was designed using a two-step synthesis procedure. First a nominal controller synthesis ensures performance of the closed loop system when the input nonlinearity is not "excited". Then, the anti-windup compensator is designed in order to guarantee the absolute stability of the closed loop system when the sector bounded nonlinearity is "excited". Numerical experiments demonstrate the effectiveness of the approach.

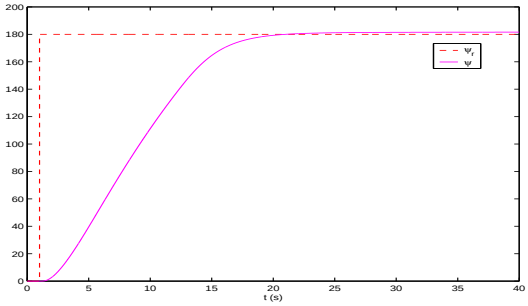

Figure 15: Heading ψ step response.

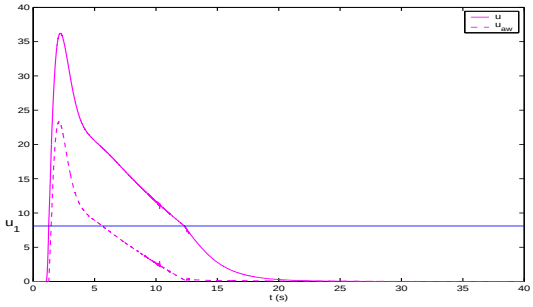

Figure 16: Control signals u and u_{aw} step response.

References

[1] G. Conte, and A. Serrani. Robust control of a remotely operated underwater vehicle. *Automatica*, vol. 34, pp. 193-198, 1988.

[2] J.-P. Folcher, and J. Rendas. Identification and control of the Phantom 500 body motion. In *Proceedings of Oceans'01*, Hawai, 2001.

[3] J.P. Folcher. Robust Design Framework for an Underwater Vehicle Motion Controller, In *Proceedings IEEE of Oceans*, pages 173–179, Biloxi, November 2002.

[4] T.I. Fossen. *Guidance and Control of Ocean Vehicles.* John Wiley & Sons, december 1995.

[5] I. Kaminer, A. Pascoal, C. Sylvestre and P. Khargonekar. Control of an underwater vehicle using $\mathbf{H}_\infty$ synthesis. In *Proceedings 30th IEEE Conference on Decision and Control*, Brighton, December, 1991.

[6] H. K. Khalil. *Nonlinear Systems.* Prentice Hall, second edition, 1996.

[7] J.-J.- Slotine, and W. Li. *Applied Nonlinear Control.* Prentice-Hall, Englewood Cliffs, 1991.